ELSEVIER

Tectonophysics 355 (2002) 145–161

TECTONOPHYSICS

www.elsevier.com/locate/tecto

The effect of crustal anisotropy on reflector depth and velocity determination from wide-angle seismic data: a synthetic example based on South Island, New Zealand

N.J. Godfrey [a,*], N.I. Christensen [b], D.A. Okaya [a]

[a] *Earth Science Department, University of Southern California, Los Angeles, CA 90089, USA*
[b] *Department of Geology and Geophysics, University of Wisconsin, Madison, WI 53706, USA*

Received 25 September 2000; received in revised form 1 June 2001; accepted 7 June 2001

Abstract

When deriving velocity models by forward modelling or inverting travel time arrivals from seismic refraction data, a heterogeneous but isotropic earth is usually assumed. In regions where the earth is not isotropic at the scale at which it is being sampled, the assumption of isotropy can lead to significant errors in the velocities determined for the crust and the depths calculated to reflecting boundaries. Laboratory velocity measurements on rocks collected from the Haast Schist terrane of South Island, New Zealand, show significant (up to 20%) compressional (P) wave velocity anisotropy. Field data collected parallel and perpendicular to the foliation of the Haast Schist exhibit as much as 11% P-wave velocity anisotropy. We demonstrate, using finite-difference full-wavefield modelling, the types of errors and problems that might be encountered if isotropic methods are used to create velocity models from data collected in anisotropic regions. These reflector depth errors could be as much as 10–15% for a 10-km thick layer with significant (20%) P-wave velocity anisotropy. The implications for South Island, New Zealand, where the problem is compounded by extreme orientations of highly anisotropic rocks (foliation which varies from horizontal to near vertical), are considered. Finally, we discuss how the presence of a significant subsurface anisotropic body might manifest itself in wide-angle reflection/refraction and passive seismic datasets, and suggest ways in which such datasets may be used to determine the presence and extent of such anisotropic bodies.

Keywords: New Zealand; Anisotropy; Seismic reflectors; Seismic velocity

1. Introduction

P- (compressional) and/ or S- (shear) wave velocity models are typically obtained from seismic refraction data by identifying relevant seismic phases, picking their travel times and using these times and sometimes the amplitudes of refracted arrivals to derive a velocity model that fits the data. The refraction velocity model is used to spatially locate reflection travel times to determine the depth and shape of impedance contrasts in the model. Such velocity models are then interpreted lithologically by comparing model velocities with velocities of candidate lithologies measured in the laboratory at appropriate temperatures and

* Corresponding author. Present address: Landmark EAME, Hill Park South, Springfield Drive, Leatherhead, Surrey, KT22 7NL, UK. Tel.: +44-1372-868737; fax: +44-1372-868601.
E-mail address: nikki_stefan@faulkners.fsworld.co.uk (N.J. Godfrey).

0040-1951/02/$ - see front matter © 2002 Elsevier Science B.V. All rights reserved.
PII: S0040-1951(02)00138-5

pressures (Birch, 1958; Christensen and Mooney, 1995).

Laboratory measurements made with relatively high frequencies on relatively small cores (centimetre scale) of Haast Schist from South Island, New Zealand, reveal significant (up to 20%) P-wave velocity anisotropy (Fig. 1). This is the maximum anisotropy possible for a large (kilometre scale) body made up of the same rock type. If foliation and other structures within a thick, large anisotropic body are uniformly oriented on a scale of hundreds of metres to kilometres, the same large amount of anisotropy measured in laboratory cores may also be detectable by lower-frequency seismic data typical of crustal scale seismic experiments. If the internal structure of the anisotropic body is less uniform, the amount of anisotropy detected by the seismic waves will be less than that measured in laboratory cores.

The Southern Cross field experiment in 1996 set out to determine whether the anisotropy of the Haast Schist measured in the laboratory is detectable in seismic data using frequencies typical of crustal scale seismic experiments. Wide-angle reflection/refraction (WAR/R) data were collected parallel and perpendicular to the near-vertical foliation of the Haast Schist (Smith, 1999) (Fig. 2a). Models derived from the Southern Cross data show that up to 11% P-wave velocity anisotropy is detectable in data collected over the Haast Schist terrane (Smith, 1999).

Two analysis methods are commonly used to derive velocity models from travel times. Ray tracing (after the method of Červený, 1972; Langan et al., 1985; Gajewski and Pšenčík, 1987; Virieux and Farra, 1991; Guest and Kendall, 1993; Qin and Schuster, 1993; Grechka and McMěchan, 1996) is a forward-modelling technique while methods based on finite-difference travel time solvers (e.g., Vidale, 1988, 1990; Eaton, 1993; Faria and Stoffa, 1994a; Aldridge and Boneau, 1996) are often used in inversion schemes such as those by Zelt and Smith (1992), Hole (1992), Lutter et al. (1993) and Hole and Zelt (1995). Travel times and amplitudes can be forward modelled using finite-difference full-waveform techniques (e.g., Virieux, 1986; Levander, 1988; van Trier and Symes, 1991; Dellinger, 1991a,b; Faria and Stoffa, 1994b; Igel et al., 1995). Both finite-difference travel time solvers and forward model ray-tracing methods that include anisotropy exist (Gajewski and Pšenčík, 1987; Dellinger, 1991a,b; Eaton, 1993; Guest et al., 1993; Qin and Schuster, 1993; Faria and Stoffa, 1994b; Igel et al., 1995; Aldridge and Boneau, 1996; Grechka and McMěchan, 1996), but are not routinely used to model WAR/R data.

If WAR/R data collected over anisotropic crust are analysed using techniques that assume an isotropic crust, travel time mismatches between near-vertical and wide-angle rays that have passed through the same subsurface region are expected. WAR/R data are, therefore, ideal for studying anisotropy and can be used to demonstrate that anisotropy needs to be incorporated into models in order to obtain good fits. In this paper, we use laboratory velocities of rocks from South Island, New Zealand, to investigate the effect of P-wave velocity anisotropy on WAR/R data by generating a synthetic seismic dataset. The parameters used to generate the synthetic data include both the intrinsic anisotropy measured in the Haast Schist as well as the anisotropy imposed due to the geometry of the schists whose foliation varies from horizontal to near-vertical. We then analyse the synthetic data as if it were field data using conventional methods that assume a heterogeneous but isotropic earth. The resulting velocity models are compared with the initial (control) parameters to understand the effect of not taking into account the material anisotropy. The results we present are particularly important in the light of two active-source seismic transects collected across South Island as part of the South Island GeopHysical Transect (SIGHT) experiment (Fig. 2a).

2. Crustal anisotropy

The mantle exhibits significant anisotropy, particularly at plate boundaries where shearing within the mantle results in the alignment of anisotropic olivine crystals (Hess, 1964; Backus, 1965; Vinnik et al., 1992). In some regions, a significant amount of anisotropy may also exist within the crust (Godfrey et al., 2000).

High-grade metamorphic rocks such as schists are usually anisotropic on the scale of laboratory cores with the fast direction parallel to foliation (Brocher et al., 1989; Brocher and Christensen, 1990; Okaya et

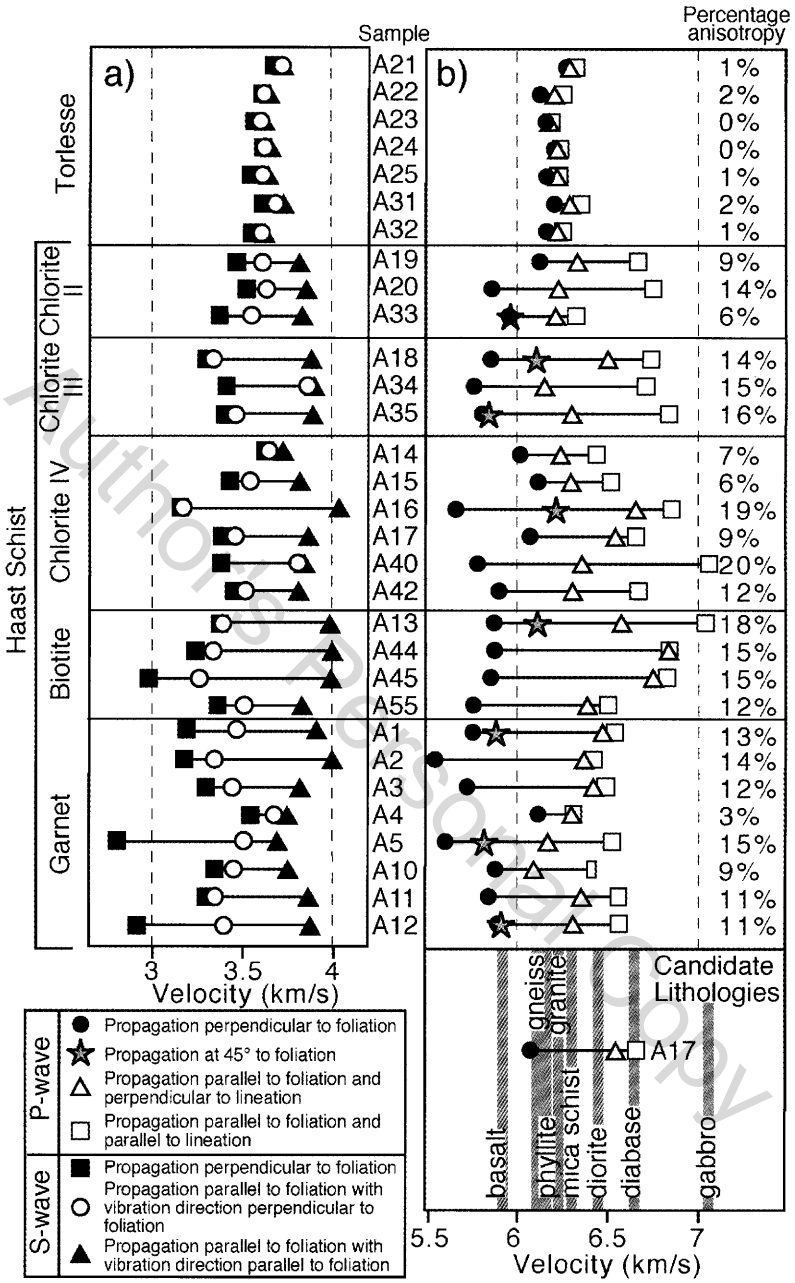

Fig. 1. Petrophysically measured velocities for the South Island, New Zealand. (a) S-wave velocities measured at a pressure of 6 kbar. (b) P-wave velocities measured at a pressure of 6 kbar. Percent P-wave anisotropy is calculated from maximum velocity minus minimum velocity divided by the average of the three orthogonal velocities. Velocities of other lithologies (at 6 kbar) are shown at the bottom as vertical bars (Christensen and Mooney, 1995).

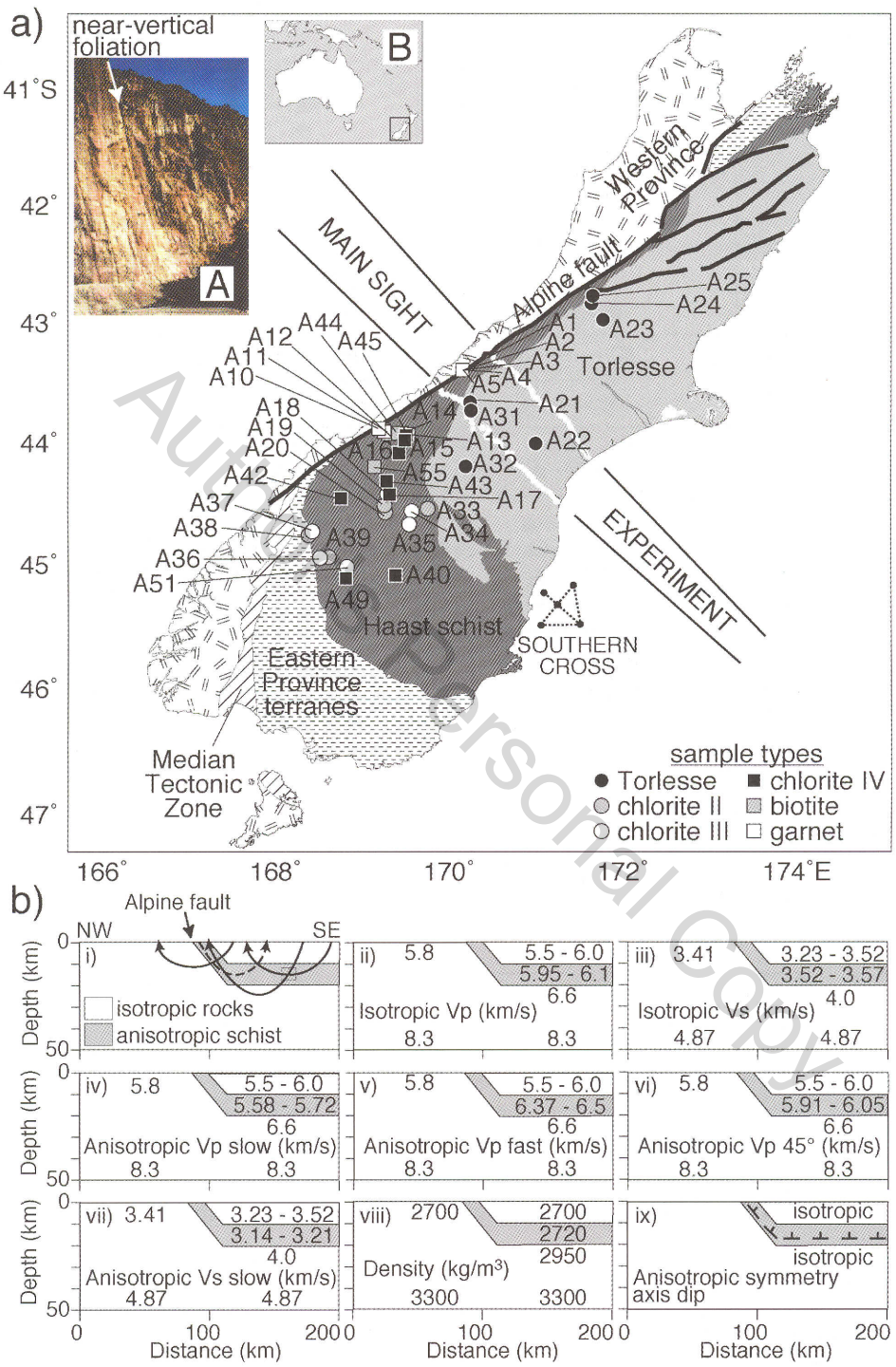

al., 1995; Godfrey et al., 2000). This anisotropy, which persists at pressures exceeding those required to close microcracks, is due to mineral alignment. Such high-grade rocks are most commonly found at mid- and lower crustal levels and are only exhumed at the surface during collisional or core complex extensional events.

Low-grade metamorphic rocks and rocks such as shales are also significantly (20–30%) transversely isotropic with the symmetry axis perpendicular to bedding (Levin, 1979; Jones and Wang, 1981; Banik, 1984). Anisotropy in shales is due to the preferred alignment of clay minerals (Johnston and Christensen, 1995) and ductile organic materials such as kerogen (Vernik and Nur, 1992). The petroleum industry routinely includes anisotropy in conventional seismic reflection data processing such as normal move-out methods (e.g., Alkhalifah and Tsvankin, 1995) and migration algorithms (e.g., Sena and Toksőz, 1993; Alkhalifah, 1995).

The inclusion of anisotropy when modelling crustal scale WAR/R data is rarely done even though the crust as a whole may be significantly anisotropic. Instances where anisotropy has been inferred from crustal scale seismic reflection and/ or refraction data include work by Brocher et al. (1989), Brocher and Christensen (1990), Carbonell and Smithson (1991a,b) and Jones et al. (1996, 1999).

Shallow crustal anisotropy attributed to phyllites of the Valdez group was modelled from data collected in southern Alaska (Brocher et al., 1989; Brocher and Christensen, 1990). A kink in the surface geometry of the shallow, high-resolution reflection/refraction seismic line allowed one subsurface region to be sampled at two azimuths. P-wave velocity anisotropy of 14% was modelled for line segments 45° apart, consistent with 20% anisotropy for orthogonal components measured in the laboratory on cores taken from Valdez group phyllites (Brocher et al., 1989; Brocher and Christensen, 1990).

Two perpendicular deep, near-vertical incidence seismic reflection lines from the Basin and Range province (USA) showed different reflectivity character which was best matched using synthetic seismograms generated with 2-D elastic finite-difference code and an anisotropic model of aligned elongated lenses in the mid- and lower crust (Carbonell and Smithson, 1991a,b).

Jones et al. (1996) determined average crustal anisotropy north of Scotland in a region with no laboratory velocity data by using the fact that the Moho in a velocity model determined from WAR/R data using an isotropic inversion technique showed a significant mismatch with the clear Moho reflection from a coincident normal incidence deep-reflection dataset. A second velocity model derived from the WAR/R data using an anisotropic inversion method with the requirement that the normal incidence Moho and WAR/R Moho matched required an average crustal anisotropy of 7%. The velocity model derived from the anisotropic WAR/R data using an isotropic technique has a 4-km Moho depth error for 25–27-km thick crust (Jones et al., 1996).

Jones et al. (1999) investigated errors arising from using isotropic methods to create a velocity model by inversion of anisotropic data by looking at P-wave Moho reflections and mantle refractions and their effect on crustal thickness and average crustal velocity determination. We take their work one stage further and look at a more complex crustal model based on South Island, New Zealand, in which both the intrinsic anisotropy of crustal material and anisotropy imposed by the geometrical arrangement of the anisotropic material are included.

3. South Island, New Zealand

The two most extensive terranes southeast of the Alpine fault (the Pacific–Australian plate boundary in

Fig. 2. (a) Terrane map of South Island, New Zealand, showing petrophysical sample locations. Inset A is a photo showing the near-vertical foliation of the Haast schist near the Alpine fault. Inset B is a location map for South Island, New Zealand. (b) Theoretical cross-section through South Island along the main SIGHT transects. (i) Example ray paths. Box shows region of the subsurface sampled by rays with different orientations. Dashed ray turns so as to remain within the fast direction of the tilted anisotropic material. (ii)–(ix) Physical parameters used for finite difference generation of synthetic seismic gathers. Velocity ranges (e.g., 5.5–6.0) represent velocities at the top and bottom of the layer respectively (linear gradient).

this region) are the Torlesse greywacke and Haast Schist terranes (Fig. 2a). Torlesse greywacke is interpreted as accretionary prism material (Howell, 1980) and is underlain by Haast Schist, which is metamorphosed Torlesse greywacke that has been exhumed from mid- and lower crustal depths at the Alpine fault (Howell, 1980). Rock samples obtained from over 50 localities were used to obtain petrophysical velocity measurements (Godfrey et al., 2000) at various pressures (depths).

3.1. Petrophysics of the Torlesse and Haast Schist terranes

For each Torlesse and Haast Schist sample, three 5-cm long, 2.54-cm diameter cores were cut in mutually perpendicular directions (perpendicular and parallel to the major foliation if present). P- and S-wave velocities were measured through each core at pressures up to 1 GPa (~ 35-km depth) using a pulse transmission technique (Christensen, 1985; Godfrey et al., 2000) (Fig. 1). For nine of the schists, P-wave velocities were also measured through a core cut at 45° to the foliation (Fig. 1b).

Torlesse greywackes are approximately isotropic (Fig. 1b). Haast Schist samples are significantly anisotropic (Fig. 1b), which at pressures exceeding those required to close microcracks is due to the preferred alignment of metamorphic minerals. Haast Schist samples have two fast P-waves (propagation parallel to foliation) and one slow P-wave (propagation perpendicular to foliation) (Fig. 1b). There are two slow S-waves (the slowest is for propagation perpendicular to foliation and the other is for propagation parallel to foliation with particle motion perpendicular to foliation) and one fast S-wave (propagation parallel to foliation with particle motion within the foliation) (Fig. 1a).

The Haast Schist samples are actually orthorhombic in symmetry, but since the models we create are two-dimensional, we only need velocity parameters that satisfy the two-dimensional form of transverse isotropy. Certain samples (e.g., samples A-1, A-2, A-3, A-4, A-36, A-37, A-44, A-45 and A-49) can be approximated to transverse isotropy by averaging the two fast P-wave and two slow S-wave velocities in order to produce the five velocities required to calculate the (five) transverse isotropic elastic constants. The two-dimensional form of transverse isotropy only requires four velocity measurements since the S wave vibrating out of the two-dimensional plane (fastest S wave, Fig. 1a) cannot exist.

3.2. Active-source seismic data from South Island

The significant anisotropy measured in Haast Schist samples is important in the light of a seismic WAR/R experiment conducted across South Island in 1996 (Davey et al., 1997). Southeast of the upturned schists adjacent to the Alpine fault, Haast Schist is believed to exist at mid- to lower crustal levels beneath the isotropic Torlesse greywackes, with approximately horizontal foliation (Wellman, 1979; Woodward, 1979; Allis, 1986). In a case such as this, near-vertical and wide-angle rays passing through the same anisotropic subsurface region sample different velocities. In the region outlined by the box in Fig. 2bi, a vertical ray samples the slow direction, a horizontal ray samples the fast direction, and a ray travelling at an intermediate angle samples an intermediate velocity. Most likely, a cumulative combination of these occurs along a ray path. On South Island, in addition to the intrinsic anisotropy of the schists, there is anisotropy imposed on the system due to the geometrical arrangement of the schist. Where Haast Schist is exposed adjacent to the Alpine fault, it has near vertical foliation (Fig. 2a, inset A). The orientation of the anisotropic medium changes faster than the orientation of the seismic ray path. The steep dip of the schist at the surface also allows the possibility that energy could be channelled along the foliation direction (fast) to receivers at the surface (dashed ray, Fig. 2bi).

4. Synthetic seismic data

We generate a synthetic dataset representing the scale and geometry of crustal scale WAR/R experiments by using a full-wavefield finite-difference method (Okaya et al., 2000). We create two synthetic seismic datasets using a two-dimensional model based on a theoretical cross-section through South Island (Fig. 2b). The first serves as a control and is generated from a fully isotropic set of parameters while the second is generated using anisotropic parameters within the layer representing the Haast Schist with

isotropic parameters elsewhere. The control dataset is used to test how well isotropic modelling techniques can recover the original (control) isotropic parameters. We ideally should be able to recover these parameters, but if we cannot due to limitations of the modelling technique, this will quantify the modelling limitation that will also be present in the analysis of the anisotropic data. Such limitations should not be confused with the effects of creating a velocity model from anisotropic data using an isotropic method.

Both earth models are 200 km long, 50 km deep and are gridded with 50-m square cells to avoid numerical dispersion. Both models include a 10-km thick layer representing the Haast Schist. Southeast (right) of model coordinate 110 the Haast Schist layer is horizontal at 10- to 20-km depth. This layer upturns to become steeply dipping in the centre of the model and crops out at the surface between model coordinates 90 (Alpine fault) and 100 (Fig. 2b). The top and bottom of the Haast Schist layer have impedance contrasts in both initial models. The upturned section of the Haast Schist layer is in the centre of the model to maximise ray coverage through the most complex part of the model. A series of synthetic seismic shot gathers were generated simulating a shot every 10-km, plus an extra shot at model coordinate 95, within the surface exposure of Haast Schist. Receivers were simulated every 250 m such that each gather consists of 800 traces. Equivalent sets of gathers for both the isotropic and anisotropic models were generated. Since our aim was to model the P-wave arrivals, we chose not to output the S-wave phases in order to simplify the gathers.

The only differences between the two earth models are the velocity parameters within the Haast Schist layer. The Haast Schist layer in the anisotropic model includes the four velocities required to describe transverse isotropy in two dimensions plus density. The velocities and densities are based on the laboratory measurements at appropriate pressures. The fast P-wave velocity parameter is that measured parallel to foliation (which is parallel to the Haast Schist layer), and the slow P-wave velocity parameter is that measured perpendicular to foliation (Fig. 2biv and v). The intermediate P-wave velocity parameter is that measured at 45° to the foliation (Fig. 2bvi). The S-wave velocity parameter is defined by S-wave propagation perpendicular to foliation with vibration direction parallel to foliation. In addition, the method used to generate the synthetic seismic data (Okaya et al., 2000) includes the ability to arbitrarily tilt the symmetry axis of an anisotropic medium within each cell. We therefore tilt the symmetry axis of the Haast Schist layer from vertical in the horizontal section of the Haast Schist to near horizontal at the Alpine fault, consistent with structural geology (Fig. 2bix).

The fully isotropic control model requires only three parameters, P-wave velocity, S-wave velocity and density (Fig. 2bii, iii and viii). We choose to use the average P-wave velocity derived from the fast and slow P-wave velocities of the anisotropic model and we use an S-wave velocity derived from the slow S-wave parameter in the anisotropic model and a typical Haast Schist fast S-wave velocity (even though the two-dimensional transverse isotropy case does not use the fast S-wave parameter).

The resulting synthetic gathers show that refractions travelling through the Haast Schist layer in the control isotropic model (black, Fig. 3) arrive later than those travelling through the Haast Schist layer in the anisotropic model (red, Fig. 3).

5. Velocity models derived from the synthetic seismic data

We picked P-wave travel times from the two synthetic seismic datasets and derived velocity models using two standard isotropic techniques; inversion of first arrivals (Hole, 1992) and associated imaging of reflections (Okaya et al., 1998), and forward modelling by interactive ray tracing (Luetgert, 1992). We first analyse the isotropic dataset to test how well our isotropic techniques can recover the control P-wave parameters. We cannot expect to do better than this with the anisotropic dataset. We then use the anisotropic dataset to determine the effect of modelling an anisotropic dataset using isotropic techniques.

5.1. Inversion method results

The first arrival travel time picks from both datasets were inverted using tomographic code of Hole (1992) with 1-km square cells and a one-dimensional starting model with a uniform velocity gradient. The amount of smoothing in the x-and z-directions was reduced every third iteration until at 24 iterations the

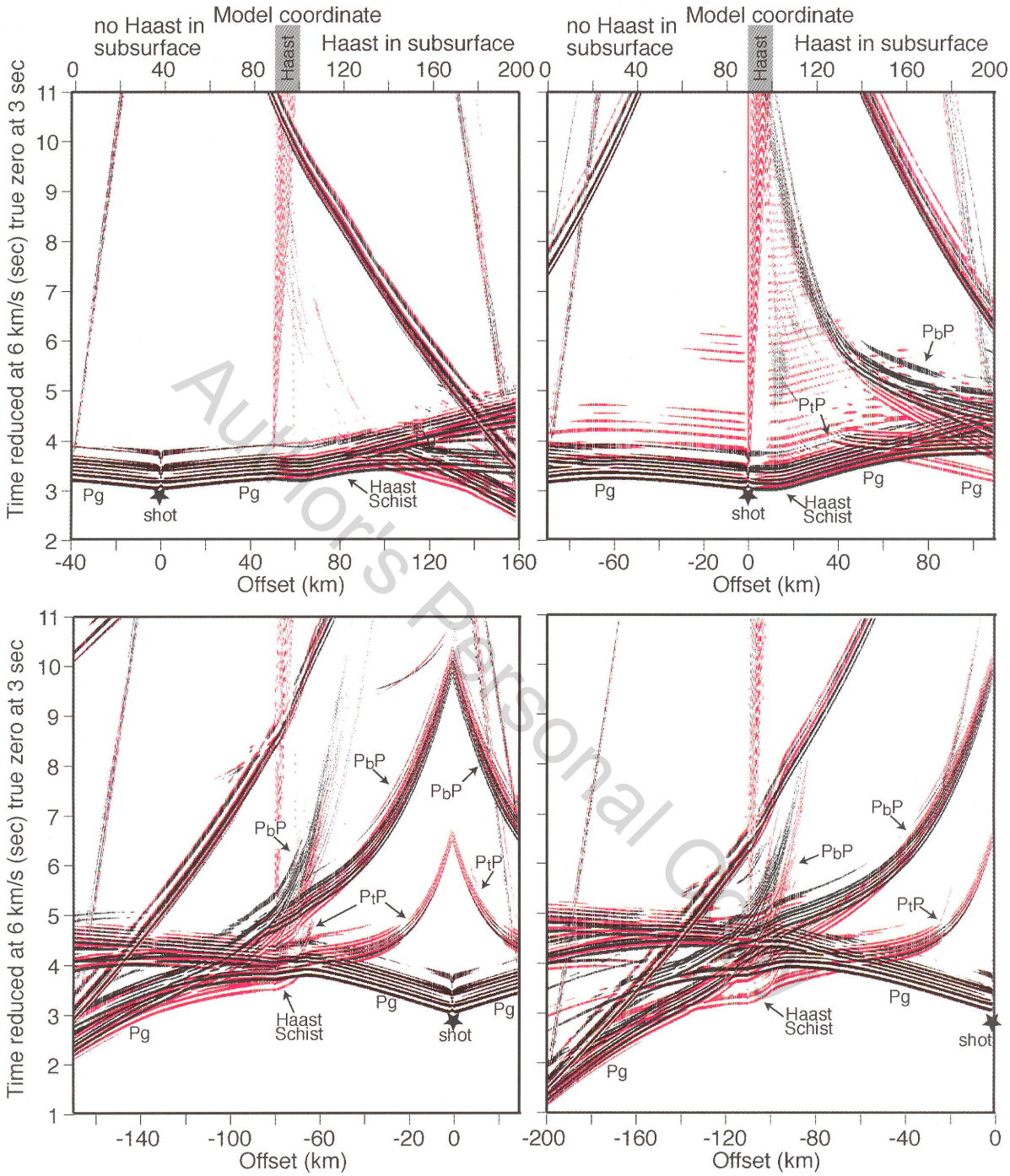

Fig. 3. Examples of synthetic seismic data generated from the control isotropic parameters (black) and anisotropic parameters (red). The phases picked and modelled are P_g (crustal refraction), P_bP (base-of-Haast reflection) and P_tP (top-of-Haast reflection).

inversion used no smoothing, i.e., 1-km smoothing over 1-km cells. The model derived from the isotropic dataset converges to low root–mean–squared (RMS) misfit values faster than the model derived from the anisotropic dataset and ultimately can be modelled with the lowest RMS misfit. The models we present in Fig. 4a have similar RMS misfit values. The isotropic inversion model (iteration 29) has an RMS misfit of 0.017 s and the anisotropic inversion model (iteration 38) has an RMS misfit of 0.019 s. The model fit to the travel times picked from the synthetic data is shown in Fig. 5.

An 'image' of the reflecting boundaries in depth is obtained by using a Kirchoff migration method on

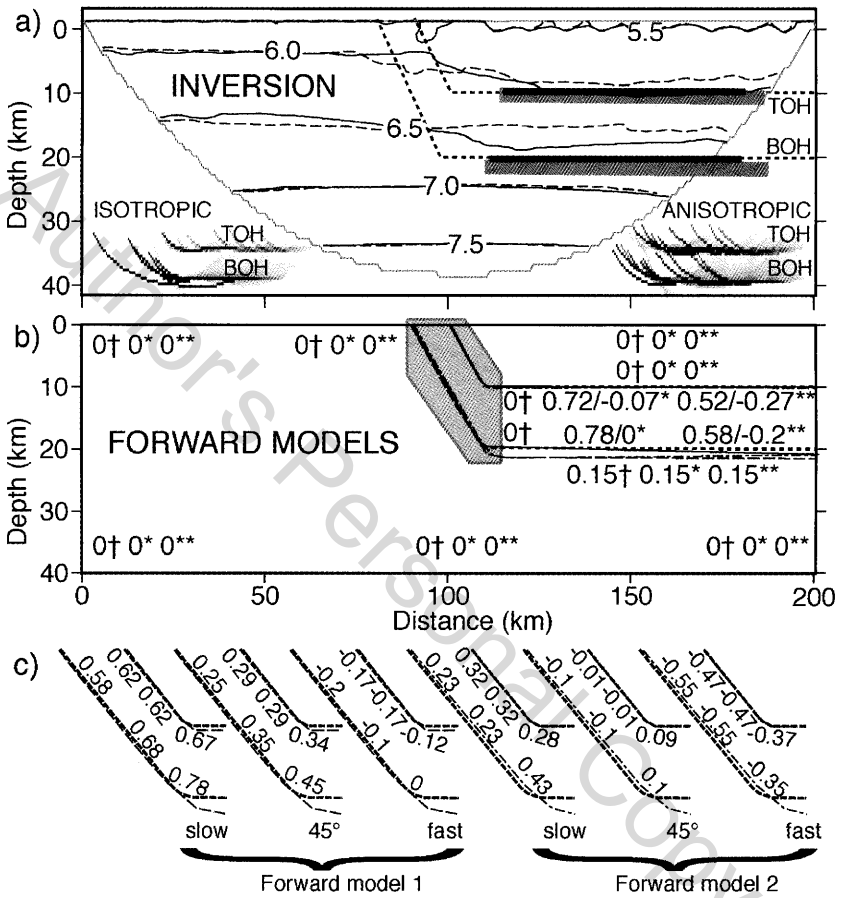

Fig. 4. P-wave velocity models derived using travel times from the synthetic seismic datasets. Dotted lines show the top (TOH) and bottom (BOH) of the Haast Schist layer in the initial models (Fig. 2). (a) Results from tomographic inversion. Numbers are P-wave velocities in kilometers per second. Isotropic model shown by solid contour lines; anisotropic model shown by dashed contour lines. Thin grey line shows the boundary of the region constrained by ray coverage. Insets show the Kirchoff migration images (reduced in size) of the reflectors. The TOH and BOH reflectors taken from the migration images are shown by bold black lines (isotropic model) and thick grey lines (anisotropic model). (b) Velocity models derived from ray-trace forward modelling. Numbers are P-wave velocity differences (ΔV) with respect to the control parameters in kilometers per second. Dagger denotes isotropic model with respect to the isotropic control model. Single asterisk denotes forward model 1 and double asterisk denotes forward model 2, both with respect to the slow and fast control velocity parameters (slow/fast). Reflectors in the isotropic forward model are shown by solid lines, and in anisotropic models 1 and 2 by dashed and dot-dashed lines, respectively. (c) Enlarged sections of the anisotropic models [see grey box in part (b)]. The isotropic model matches the isotropic control model exactly and is not shown. Values are ΔV (km/s) for forward models 1 and 2 with respect to the slow, 45° and fast initial P-wave velocities.

the reflection travel times through the velocity model derived from the refraction data. If the velocity model is correct in terms of the reflection raypaths, the image of the reflecting boundary will be at the correct depth and will appear focused. If the velocity model is incorrect, the image of the reflecting

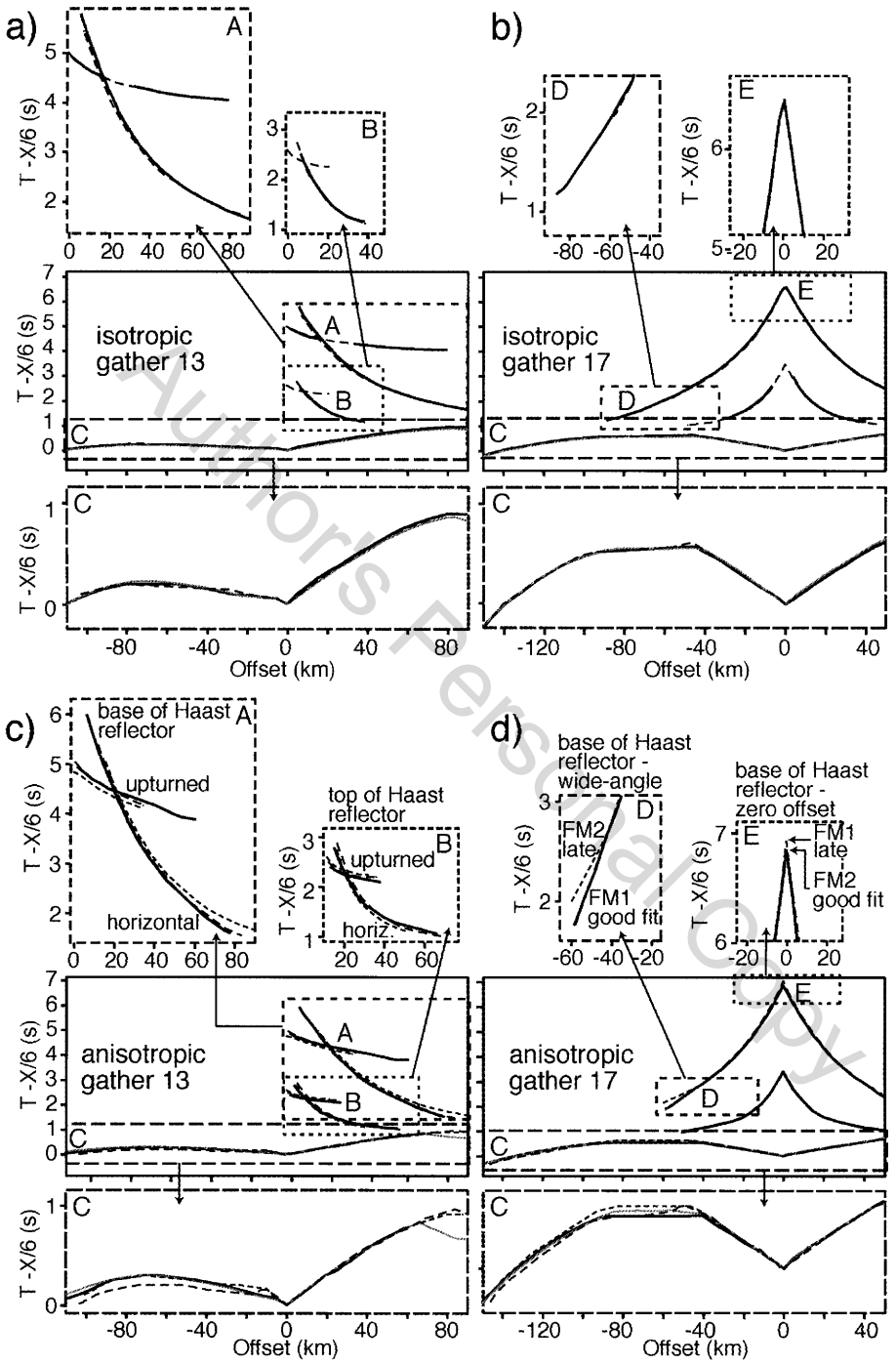

boundary will be diffuse, and its depth may be incorrect.

5.1.1. Results from the isotropic dataset

The inversion was able to reproduce the velocities above, beneath and northwest of the Haast Schist layer, and was able to correctly locate the top of Haast (TOH) and base of Haast (BOH) reflectors southeast of model coordinate 115 km (focussed image, inset left, Fig. 4a). The inversion was not able to image the upturned section of Haast Schist correctly in terms of lateral location, velocity or reflector image. The horizontal section of the Haast Schist layer is slightly faster (up to 9%) than the initial model. The velocity inversion at the TOH boundary is not reproduced. We can not expect to do better than this with the anisotropic dataset.

5.1.2. Results from the anisotropic dataset

Although the overall RMS misfit for the anisotropic inversion model is similar to that for the isotropic inversion model, locally misfits are larger (Fig. 5c and d). Ignoring the errors due to the limitations of the analysis technique, the inversion of anisotropic first arrivals results in P-wave velocities at the top of the Haast Schist layer that are close to, but slower than the fast P-wave parameters of the anisotropic control model. P-wave velocities at the base of the Haast Schist layer are faster than the fast P-wave parameters of the control model (Fig. 4a). The horizontal section of the TOH and BOH boundaries at 10–11-km depth (up to 1 km deeper than the anisotropic control model) and 21–23-km depth (1–3 km deeper than the anisotropic control model), respectively (inset right, Fig. 4a), are imaged as poorly focussed features. This suggests that the anisotropic inversion model velocities above and within the Haast Schist layer are fast with respect to the reflection paths.

5.2. Forward modelling results

We also derived velocity models from each dataset using forward-modelling, interactive ray tracing (Luetgert, 1992) in which we aimed to match the travel times of both reflections and refractions in the data. This technique allows for velocity discontinuities, unlike the smooth inversion models described above.

5.2.1. Results from the isotropic dataset

The P-wave velocity model derived from the isotropic dataset (Fig. 4b) exactly reproduces the isotropic control parameters except for the slightly higher (2%) velocity immediately below the Haast schist layer. We have reproduced the upturned section of Haast Schist, the velocity inversion at the 10-km deep TOH boundary and the 20-km deep BOH boundary. The model fit to the data is good for both refractions and reflections (Fig. 5a and b).

5.2.2. Results from the anisotropic dataset

It is not possible to obtain as good a fit to the anisotropic data as we achieved for the isotropic data by forward modelling. We present two alternative models (1 and 2) (Fig. 4b) that match the travel times of different parts of the dataset (Fig. 5c and d). Velocities in the northwest part of the model (model coordinates 0–90) and above the Haast Schist layer match the anisotropic control parameters. The region beneath the Haast Schist is 2% faster than the control model, but is the same as the isotropic forward model.

The model fit to the data for anisotropic forward model 1 is reasonable for refractions at all offsets (Fig. 5cC and dC), reasonable for reflections off the TOH boundary near the upturned section (Fig. 5cB), good for reflections at all offsets off the horizontal section of the TOH boundary and good for wide-angle reflections off the BOH boundary (Fig. 5dD). Zero-offset

Fig. 5. Forward ray trace and inversion model arrival times plotted against travel times picked from the synthetic data (solid black lines) for two gathers. Grey lines are arrival times for the inversion models. Long dashed lines are ray-traced arrival times for the isotropic forward model and anisotropic forward model 1. Short dashed lines are ray-traced arrival times for anisotropic forward model 2. Times are all reduced at 6 km/s. For each example (a)–(d), the entire gather is shown in the centre, a vertically exaggerated section showing refractions is shown below (C) and vertically exaggerated sections showing reflections are shown above (A, B, D and E). (a) Isotropic shot gather whose source is located at model coordinate 110. (b) Isotropic shot gather whose source is located at model coordinate 150. (c) Anisotropic shot gather whose source is located at model coordinate 110. (d) Anisotropic shot gather whose source is located at model coordinate 150.

and near-vertical reflections off the BOH boundary in the model arrive later than those in the data (Fig. 5dE). The upturned section of Haast Schist is reproduced fairly well, although it is slightly (6%) thicker than the anisotropic control model (Fig. 4c). The velocities within the horizontal section of the Haast Schist layer are close (within 1%) or equal to the fast P-wave velocity parameters of the anisotropic control model. The BOH boundary is at 22.2-km depth, 11% deeper than the anisotropic control model.

The model fit to the data for anisotropic forward model 2 is reasonable for refractions at all offsets (Fig. 5cC and dC), reasonable for reflections off the TOH boundary near the upturned section (Fig. 5cB), good for reflections at all offsets off the horizontal section of the TOH boundary and good for near-vertical and zero-offset reflections off the BOH boundary (Fig. 5dE). Wide-angle reflections off the BOH boundary in the model arrive later than those in the data (Fig. 5dD). The upturned section of Haast Schist is reproduced fairly well, although it is slightly thinner (5%) than the anisotropic control model (Fig. 4c). Velocities within the horizontal section of the Haast Schist layer are slower than anisotropic forward model 1, but still closer to the fast P-wave velocity parameters of the anisotropic control model than the slow P-wave velocity parameters. The BOH boundary is at 21.8–22.2-km depth, dipping northwest, 9–11% deeper than the anisotropic control model.

5.3. Summary

It is not possible to create a single model that fits both refractions and reflections from the anisotropic dataset at all offsets. Our modelling shows the refraction data gives velocities close or equal to the fast control anisotropic velocity parameters, and if these velocities are used to model reflectors that are beneath the anisotropic body, the reflectors may appear up to 15% deeper than their true depth.

6. Discussion

Our models include the effects of both the intrinsic anisotropy of the schists (the horizontal section of the Haast Schist layer in which the foliation is horizontal) and the anisotropy imposed on the system by geometry (where the Haast Schist layer tilts so that the foliation changes from horizontal to steeply dipping).

6.1. Intrinsic anisotropy

Three issues arise from modelling data collected in a region with only intrinsic anisotropy using isotropic techniques. (1) It is not possible to fit the travel times of reflection phases at all offsets with a single model. (2) Velocity models derived from refraction phases are biased towards the horizontal velocity parameter. (3) Depths to reflecting boundaries determined primarily from near-vertical reflections will be incorrect if the velocity model used to locate them is based on refractions in the same dataset.

6.1.1. Reflection travel times

It is not possible to fit both near-vertical and wide-angle reflections beneath an anisotropic region with a single model. Both near-vertical and wide-angle reflections sample the same velocities in an isotropic dataset if generated from a one-dimensional velocity field (equivalent to our model between model coordinates 110 and 200). Near-vertical and wide-angle reflections travelling through an equivalent anisotropic layer sample different velocities. A velocity model close to the horizontal velocity parameter will fit the long-offset part of the travel time curve, while a different velocity model close to the vertical velocity parameter is required to fit the short-offset part of the travel time curve.

6.1.2. Velocity models

Velocity models derived from modelling refraction phases are biased towards the horizontal velocity parameter. Refraction rays travel with a wide range of orientations from near vertical close to the source and receiver to horizontal where the ray turns deeper in the crust or mantle. Velocity models are best constrained where refraction rays turn. Velocity models derived from refraction phases are therefore most similar to the horizontal velocity parameter, rather than the average velocity, which might be the case if all ray orientations contributed equally to the model. By contrast, velocity models derived from teleseismic earthquake arrivals, which have near-vertical paths through the crust, will be biased towards the vertical velocity parameter.

Models biased towards fast or slow velocities due to the presence of anisotropic material may be misinterpreted in terms of lithology. Petrophysical data are often published as average velocity values at particular depths or pressures, even in the case of anisotropic rocks. Our petrophysical measurements on Haast Schist samples demonstrate that a single rock type can encompass a large range of velocities, e.g., Haast Schist sample A-17 has a fast P-wave velocity similar to diabase and a slow P-wave velocity similar to granite or gneiss (Fig. 1b).

6.1.3. Depths to reflecting boundaries

Depths to reflecting boundaries determined from near-vertical reflections may be incorrect if the velocity model used to locate them is based on refractions in the same dataset. The error in reflector depth for a reflector beneath or within an anisotropic body with vertical or horizontal foliation is dependent on the relative difference between the vertical velocity (V_V) sampled by near-vertical reflections and the horizontal velocity (V_H) sampled by refractions, which is directly related to percentage anisotropy (A).

$$A = 100\frac{(V_H - V_V)}{V_{average}} = 200\frac{(V_H - V_V)}{(V_H + V_V)} \quad (1)$$

The zero-offset travel time (t) to a reflecting boundary is dependent on the true depth to the boundary (Z) and vertical velocity (Fig. 6a). If this travel time is used to determine the depth to the boundary using an incorrect velocity such as the horizontal velocity obtained by modelling refraction travel times, an incorrect depth, Z_E will result (Fig. 6b).

$$t = \frac{Z}{V_V} = \frac{Z_E}{V_H} \quad (2)$$

The depth error is given by

$$\Delta Z = Z_E - Z \quad (3)$$

Eqs. (1)–(3) can be used to obtain the relationship between the normalised depth error and percentage anisotropy (plotted in Fig. 6c)

$$\frac{\Delta Z}{Z} = \frac{(200 + A)}{(200 - A)} - 1 \quad (4)$$

It should be noted that the horizontal velocity determined from refraction travel times may be slightly different from the true horizontal velocity of the medium, which will affect the exact value calculated for percentage anisotropy, which in turn affects the normalised depth error.

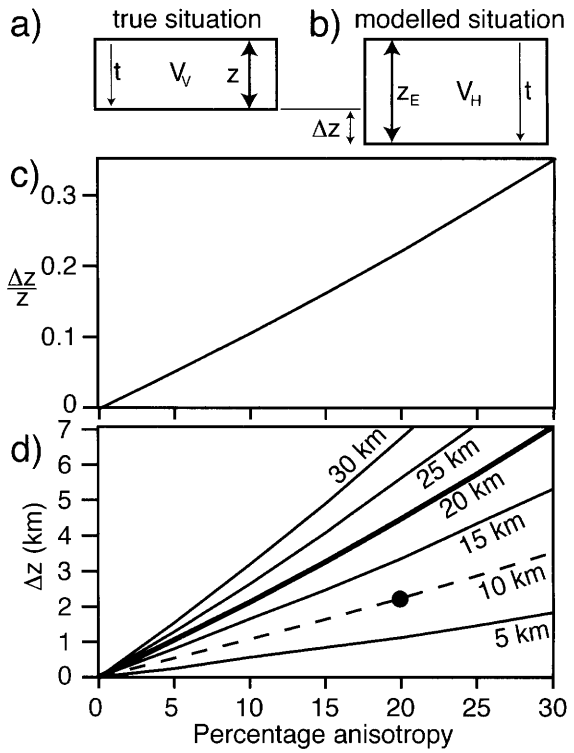

Fig. 6. Error in depth estimation due to anisotropy. (a) Schematic showing variables relevant to the true earth case. (b) Schematic showing variables relevant to the modelled case. (c) Graph showing depth error normalised to the thickness of an anisotropic layer versus percentage P-wave anisotropy. (d) Graph showing the depth error resulting from a 10-km thick (dashed) and 20-km thick (solid line) anisotropic layer versus percentage P-wave anisotropy. Circle shows the location of a 10-km thick body with 20% anisotropy—the case we modelled with synthetic seismic data.

Reflector depth errors of as much as 5 km are possible for a 20-km thick anisotropic body with ~ 20% anisotropy (Fig. 6d). A reflector beneath a 10-km thick anisotropic body with 20% P-wave velocity anisotropy could be mislocated by as much as 2.2 km (circle, Fig. 6d), consistent with our synthetic modelling results.

For more discussion on the influence of anisotropy on the travel times of near-vertical reflections and their relation to horizontal and vertical propagation velocities, see also articles by Hake and Mesdag (1984) and Helbig (1994).

6.2. Geometrically imposed anisotropy

Additional anisotropy is imposed on the system in the form of the upturned section of Haast Schist. Since the inversion could not reproduce the upturned section of the Haast Schist even for the isotropic dataset, we only discuss the results of forward modelling. The models derived from the anisotropic dataset do not accurately reproduce the thickness of the upturned section of Haast Schist. The upturned Haast Schist has an average dip of $\sim 45°$, so the horizontal velocity sampled by turning rays in the upturned region should be close to the 45° velocity parameter (Fig. 2bvi). Anisotropic forward model 1 has velocities significantly slower than the 45° velocity parameter while anisotropic forward model 2 has velocities slightly faster than the 45° velocity parameter (Fig. 4c).

7. Identification of subsurface anisotropic material on South Island, New Zealand

The foliation orientation and structural thickness of the upturned Haast Schist at the surface is known due to geological mapping. Recent studies suggest the schist layer turns in the subsurface so that its foliation becomes horizontal some distance southeast of the Alpine fault, but the exact subsurface geometry has not been identified (Wellman, 1979; Allis, 1986). The petrophysical velocity change from isotropic Torlesse greywacke to the lowest grade but highly anisotropic chlorite II zone Haast Schist is sudden (Fig. 1b). Geobarometry of chlorite II zone and garnet zone rocks now at the surface indicate the original depths of the top and base of the Haast Schist. Anisotropy is direction sensitive, so there may be seismic datasets that detect anisotropy in the crust and if so, they may be used to determine the extent, orientation and thickness of anisotropic material beneath South Island. The South Island datasets discussed below exist for future analysis.

Velocity models derived from active-source WAR/R SIGHT data (Davey et al., 1997) may appear to be inconsistent with models of the same region derived from near-vertical teleseismic arrivals recorded in a passive seismic experiment (SAPSE) (Anderson et al., 1997). A single velocity model that fits all the data using both types of data simultaneously may not be possible. A comparison of active-source velocity models along the SIGHT transects with velocity models derived from teleseismic data may indicate a substantial thickness of Haast Schist. A relatively slow velocity model might be expected from the teleseismic data (consistent with velocities measured perpendicular to foliation in the Haast Schist) while a relatively fast velocity model might be expected from the active-source data (consistent with velocities measured parallel to foliation in the Haast Schist). Examination of the model fit to the data at all offsets for reflections interpreted to travel through the Haast Schist may be used to identify anisotropic material. If a model that fits the reflection travel times equally well at all offsets cannot be found, and errors in the model caused by oversimplification, badly constrained inversion parameters or three-dimensional effects can be ruled out, anisotropic material may be present at some depth above the reflector in question. Migrating near-vertical SIGHT CDP data collected in 1998 (Henrys et al., 1998) using a velocity model derived from SIGHT WAR/R data will not produce a good image of reflectors if anisotropic material is present. A slower velocity model that better represents the vertical velocity field may produce a better migration image. Where there is anisotropic material in the subsurface, the two-way travel time of CDP reflections will not match the calculated zero-offset two-way travel time of equivalent reflectors in the velocity model derived from the WAR/R dataset.

If the contribution of shear-wave splitting in the crust can be separated out from that in the mantle, shear-wave splitting events in the teleseismic earthquake dataset may be used to determine where the Haast Schist layer turns and becomes horizontal. Shear-wave splitting in the crust is expected where the foliation of the Haast Schist is near-vertical or steeply dipping while no shear-wave splitting in the crust is expected where the Haast Schist foliation is horizontal (Godfrey et al., 2000). More information regarding the role of shear-wave splitting in constraining anisotropic subsurface models can be found in articles by Rabbel et al. (1998) and Bohlen et al. (1999).

The SIGHT and SAPSE datasets, along with the petrophysical data collected from South Island, have

the potential to address many questions concerning anisotropy related to the Haast Schist. Lessons learned from South Island, New Zealand, may then be applied to other regions of the world to try and identify and quantify subsurface anisotropic bodies.

8. Conclusions

We have shown that an anisotropic body such as the Haast Schist on South Island, New Zealand, is likely to have a significant effect on crustal scale wide-angle reflection/refraction data. Effects include velocities biased towards the horizontal velocity parameter of the anisotropic layer, and errors in the depth calculated to reflecting boundaries within or beneath an anisotropic body when a biased velocity model is used. These reflector depth errors could be as much as 10–15% for a 10-km thick layer with significant (20%) P-wave velocity anisotropy. The presence of an anisotropic layer in the subsurface may explain travel time misfits between the model and the data for reflection phases at different offsets as well as apparent discrepancies between models derived from different data types, e.g., active-source wide-angle reflection/refraction data and passive teleseismic earthquake data.

The SIGHT and SAPSE seismic and petrophysical data have the potential to address many questions concerning anisotropy. The lessons learned from South Island will be applicable to other regions of the world for identifying subsurface anisotropic bodies, or if it is known a priori that they exist, to account for them during modelling and imaging of the data.

Serious thought will be required to decide how best to efficiently and cheaply model this kind of data, but it must be taken into account and cannot be ignored. The New Zealand SIGHT and SAPSE datasets will provide an excellent opportunity to develop methods for dealing with large amounts of data in both 2-D and 3-D geometries from highly anisotropic regions in a cost effective, efficient manner.

Acknowledgements

This work was supported by National Science Foundation grant EAR-9418530.

References

Aldridge, D.F., Boneau, T.C., 1996. Finite-difference traveltime computation for transversely isotropic elastic media. SEG Annual Meeting Expanded Technical Program Expanded Abstracts with Authors Biographies, vol. 66, pp. 479–482.

Alkhalifah, T., 1995. Gaussian beam migration in anisotropic media. Geophysics 60, 1474–1484.

Alkhalifah, T., Tsvankin, I., 1995. Velocity analysis for transversely isotropic media. Geophysics 60, 1550–1566.

Allis, R.G., 1986. Mode of crustal shortening adjacent to the Alpine fault, New Zealand. Tectonics 5, 15–32.

Anderson, H., Eberhart-Phillips, D., McEvilly, T., Wu, F., Uhrhammer, R., 1997. Southern Alps Passive Seismic Experiment, vol. 97/21. Institute of Geological and Nuclear Sciences, Lower Hutt, New Zealand, 20 pp.

Backus, G.E., 1965. Possible forms of seismic anisotropy of the uppermost mantle under oceans. J. Geophys. Res. 70, 3429–3439.

Banik, N.C., 1984. Velocity anisotropy of shales and depth estimation in the North Sea basin. Geophysics 49, 1411–1419.

Birch, A.F., 1958. Interpretation of the seismic structure of the crust in the light of experimental studies of wave velocities in rocks. In: Benioff, V.H. (Ed.), Contributions in Geophysics. Pergamon, Oxford, pp. 158–170.

Bohlen, T., Rabbel, W., Weiss, T., Siegesmund, S., Pohl, M., 1999. Recovering shear-wave anisotropy of the lower crust; the influence of systematic errors on travel-time inversion. Pure Appl. Geophys. 156, 123–138.

Brocher, T.M., Christensen, N.I., 1990. Seismic anisotropy due to preferred mineral alignment observed in shallow crustal rocks in southern Alaska. Geology 18, 737–740.

Brocher, T.M., Fisher, M.A., Geist, E.L., Christensen, N.I., 1989. A high-resolution seismic reflection/refraction study of the Chugach–Peninsular terrane boundary, southern Alaska. J. Geophys. Res. 94, 4441–4455.

Carbonell, R., Smithson, S.B., 1991a. Large-scale anisotropy within the crust in the Basin and Range province. Geology 19, 698–701.

Carbonell, R., Smithson, S.B., 1991b. Crustal anisotropy and the structure of the Mohorovicic discontinuity in western Nevada of the Basin and Range province. In: Meissner, R.O., et al., (Eds.), Continental Lithosphere; Deep Seismic Reflections. American Geophysical Union, Washington, DC, pp. 31–38.

Červený, V., 1972. Seismic rays and ray intensities in inhomogeneous anisotropic media. Geophys. J. R. Astron. Soc. 29, 1–13.

Christensen, N.I., 1985. Measurements of dynamic properties of rocks at elevated pressures and temperatures. In: Pincus, H.J., Hoskins, E.R. (Eds.), Measurements of Rock Properties at Elevated Pressures and Temperatures. American Society of Testing and Materials STP869, Philadelphia, PA, pp. 93–107.

Christensen, N.I., Mooney, W.D., 1995. Seismic velocity structure and composition of the continental crust: a global review. J. Geophys. Res. 100, 9761–9788.

Davey, F.J., et al., 1997. Preliminary results from a geophysical study across a modern, continent–continent collisional plate boundary—the Southern Alps, New Zealand. Tectonophysics 288, 221–235.

Dellinger, J.A., 1991a. Anisotropic finite-difference traveltimes. Society of Exploration Geophysicists 61st International Annual Meeting, Expanded Abstracts. Society of Exploration Geophysicists, pp. 1530–1533.

Dellinger, J.A., 1991b. Anisotropic seismic wave propagation. PhD thesis, Stanford University, Stanford, CA, 173 pp.

Eaton, W.S., 1993. Finite-difference traveltime calculation for anisotropic media. Geophys. J. Int. 114, 273–280.

Faria, E.L., Stoffa, P.L., 1994a. Traveltime computation in transversely isotropic media. Geophysics 59, 272–281.

Faria, E.L., Stoffa, P.L., 1994b. Finite-difference modeling in transversely isotropic media. Geophysics 59, 282–289.

Gajewski, D., Pšenčík, I., 1987. Computation of high-frequency seismic wavefields in 3D laterally inhomogeneous anisotropic media. Geophys. J. R. Astron. Soc. 91, 383–411.

Godfrey, N.J., Christensen, N.I., Okaya, D.A., 2000. Anisotropy of schists: contribution of crustal anisotropy to active-source seismic experiments and shear-wave splitting observations. J. Geophys. Res. 105, 27991–28007.

Grechka, V.Y., McMěchan, G.A., 1996. 3-D two point ray-tracing for heterogeneous, weakly transversely isotropic media. Geophysics 61, 1883–1894.

Guest, W.S., Kendall, J.-M., 1993. Modelling seismic waveforms in anisotropic inhomogeneous media using ray and Maslov asymptotic theory; applications to exploration seismology. Can. J. Explor. Geophys. 29, 78–92.

Guest, W.S., Thomsen, C.J., Spencer, C.P., 1993. Anisotropic reflection and transmission calculations with application to a crustal seismic survey from the East Greenland Shelf. J. Geophys. Res. 98, 14161–14184.

Hake, K., Mesdag, C.S., 1984. Three term Taylor series for t (sub 2)–x (super 2) curves of P- and S-waves over layered transversely isotropic ground. Geophys. Prospect. 32, 828–850.

Helbig, K., 1994. Foundations of Anisotropy for Exploration Seismics. Elsevier, Oxford, 486 pp.

Henrys, S., Okaya, D., Melhuish, A., Stern, T., Holbrook, W.S., 1998. Near-vertical seismic images of a continental transpressional plate boundary: Southern Alps, New Zealand. EOS Trans., Am. Geophys. Union 79, F901.

Hess, H.H., 1964. Seismic anisotropy of the uppermost mantle under oceans. Nature 203, 629–631.

Hole, J.A., 1992. Non-linear high-resolution three-dimensional seismic travel-time tomography. J. Geophys. Res. 97, 6553–6562.

Hole, J.A., Zelt, B.C., 1995. 3-D finite-difference reflection traveltimes. Geophys. J. Int. 121, 427–434.

Howell, D.G., 1980. Mesozoic accretion of exotic terranes along the New Zealand segment of Gondwanaland. Geology 8, 487–491.

Igel, H., Mora, P., Riollet, B., 1995. Anisotropic wave propagation through finite-difference grids. Geophysics 60, 1203–1216.

Johnston, J.E., Christensen, N.I., 1995. Seismic anisotropy of shales. J. Geophys. Res. 100, 5991–6003.

Jones, L.E.A., Wang, H.F., 1981. Ultrasonic velocities in Cretaceous shales from the Williston basin. Geophysics 46, 288–297.

Jones, K.A., Warner, M.R., Morgan, R.P.L., Morgan, J.V., Barton, P.J., Price, C.E., 1996. Coincident normal-incidence and wide-angle reflections from the Moho: evidence for crustal seismic anisotropy. Tectonophysics 264, 205–217.

Jones, K., Warner, M., Brittan, J., 1999. Anisotropy in multi-offset deep-crustal seismic experiments. Geophys. J. Int. 138, 300–318.

Langan, R.T., Lerche, I., Cutler, R.T., 1985. Tracing of rays through heterogeneous media: an accurate and efficient procedure. Geophysics 50, 1456–1465.

Levander, A.R., 1988. Fourth-order, finite-difference P–SV seismogram. Geophysics 53, 1425–1436.

Levin, F.K., 1979. Seismic velocities in transversely isotropic media. Geophysics 44, 918–936.

Luetgert, J.H., 1992. MacRay: interactive two-dimensional seismic raytracing for the Macintosh. U.S. Geological Survey Open File Report 92-356, 43 pp.

Lutter, W.J., Trehu, A.M., Nowack, R.L., 1993. Application of 2-D travel time inversion of seismic refraction data to the mid-continent rift beneath Lake Superior. Geophys. Res. Lett. 20, 615–618.

Okaya, D., Christensen, N.I., Stanley, D., Stern, T., 1995. Crustal anisotropy in the vicinity of the Alpine fault zone, South Island, New Zealand. N.Z. J. Geol. Geophys. 38, 579–583.

Okaya, D., Godfrey, N., Pattelena, T., Henyey, T., 1998. Velocity structure of the Los Angeles region at differing spatial granularity. Contributions to the Group D 3-D Velocity Project (abstract), Southern California Earthquake Center Annual Meeting.

Okaya, D.A., Christensen, N.I., Godfrey, N.J., 2000. Elastic wave propagation in anisotropic material possessing arbitrary internal tilt. Haast schist terrane, South Island, New Zealand (abstract), Deep Seismic Profiling of the Continents and their Margins, Ulvik, Norway.

Qin, F., Schuster, G.T., 1993. First-arrival traveltime calculation for anisotropic media. Geophysics 58, 1349–1358.

Rabbel, W., Siegesmund, S., Weiss, T., Pohl, M., Bohlen, T., 1998. Shear wave anisotropy of laminated lower crust beneath Urach (SW Germany); a comparison with xenoliths and with exposed lower crustal sections. Tectonophysics 197, 337–356.

Sena, A.G., Toksőz, M.N., 1993. Kirchoff migration and velocity analysis for converted and nonconverted waves in anisotropic media. Geophysics 58, 265–276.

Smith, R.A., 1999. Macroscopic P-wave anisotropy in the Haast Schist, New Zealand: implications for errors in wide-angle seismic studies of metamorphic terranes. Masters thesis, University of Wyoming, Laramie, WY, 147 pp.

van Trier, J., Symes, W.W., 1991. Upwind finite-difference calculation of traveltimes. Geophysics 56, 812–821.

Vernik, L., Nur, A., 1992. Ultrasonic velocity and anisotropy of hydrocarbon source rocks. Geophysics 57, 727–735.

Vidale, J., 1988. Finite-difference calculation of traveltimes. Bull. Seismol. Soc. Am. 78, 2062–2076.

Vidale, J.E., 1990. Finite-difference calculation of traveltimes in three dimensions. Geophysics 55, 521–526.

Vinnik, L.P., Makeyeva, L.J., Melev, A., Usenko, A.Y., 1992. Global patterns of azimuthal anisotropy and deformation in the continental mantle. Geophys. J. Int. 111, 433–447.

Virieux, J., 1986. P–SV wave propagation in heterogeneous media: velocity-stress, finite-difference method. Geophysics 51, 889–901.

Virieux, J., Farra, V., 1991. Ray-tracing in 3-D complex isotropic media: an analysis of the problem. Geophysics 56, 2057–2069.

Wellman, H.W., 1979. An upliftmap for the South Island of New Zealand, and model for the uplift of the Southern Alps. In: Walcott, R.I., Cresswell, M.M. (Eds.), The Origin of the Southern Alps. Royal Society of New Zealand Bulletin, vol. 18, pp. 12–20.

Woodward, D.J., 1979. The crustal structure of the Southern Alps, New Zealand, as determined by gravity. In: Walcott, R.I., Cresswell, M.M. (Eds.), The Origin of the Southern Alps. Royal Society of New Zealand Bulletin, vol. 18, pp. 95–98.

Zelt, C.A., Smith, R.B., 1992. Seismic traveltime inversion for 2-D crustal velocity structure. Geophys. J. Int. 108, 16–34.